Dyes and Pigments 92 (2012) 1344–1350

Contents lists available at SciVerse ScienceDirect

Dyes and Pigments

journal homepage: www.elsevier.com/locate/dyepig

Theoretical study of charge transfer mechanism in fullerene-phenyl-phenothiazine compound: A real-space analysis

Yuanzuo Li[a,b,*], Fengcai Ma[c], Bin Dong[d], Jing Li[e], Maodu Chen[b]

[a] College of Science, Northeast Forestry University, Harbin 150040, PR China
[b] School of Physics and Optoelectronic Technology, Dalian University of Technology, Dalian 116024, PR China
[c] Department of Physics, Liaoning University, Shenyang 110036, PR China
[d] School of Science, Dalian Nationalities University, Dalian 116600, PR China
[e] Departamento de Química, Universidade de Coimbra, 3004-535, Portugal

ARTICLE INFO

Article history:
Received 1 February 2011
Received in revised form
23 August 2011
Accepted 24 August 2011
Available online 3 September 2011

Keywords:
Fullerene derivatives
Real-space analysis
Excited state
Charge transfer

ABSTRACT

Quantum chemistry methods as well as two-dimensional (2D) and three-dimensional (3D) real-space analysis have been conducted to study the photo-induced intramolecular charge-transfer (ICT) and excited state properties of fullerene-phenylphenothiazine, which has recently been developed for solar cells. Firstly, we obtained the energy levels and spatial distributions of HOMO/LUMO, energy gap (ΔE_{H-L}) and excitation energies on the basis of quantum chemistry study. Secondly, two-dimensional (2D) and three-dimensional (3D) real-space analysis were used to visualize the CT process and to reveal the nature of the excited states. In the above analyses, the 2D real-space analysis of the transition density matrix provided information about the electron-hole coherence, and the 3D real-space analysis of charge difference density enabled the visualization of the orientation and result of the ICT. The results of real-space analysis directly indicate that some states are ICT states, and others belong to locally excited states. Moreover, according to the generalized Mulliken Hush theory, we calculated the electronic coupling matrix elements and predict that electron transfer for some ICT states more easily takes place than that for some locally excited states.

© 2011 Elsevier Ltd. All rights reserved.

1. Introduction

Photo-induced charge transfer (PCT) has attracted interest widely due to potential applications in optoelectronic devices and artificial photosynthesis systems [1–3], and PCT is considered as the fundamental and crucial step in a variety of photophysical and photochemical processes. Much work has been carried out on the development of suitable donor–acceptor (D–A) systems with strong coupling and low reorganization energy in the electron-transfer reaction [4,5]. Fullerene (C60) derivatives, having unique characteristics (such as low reduction potential, small reorganization and preferable stability, etc.), have displayed excellent electron accepting ability in photo-induced CT processes [6–13]. For the fullerene-donor system, photoexcitation induces electron transfer from donor to acceptor, forming a radical anion of the donor group and a radical cation of the acceptor group, and this process is observable in nanosecond time region; thus covalently bonded C60-donor dyads and triads are generally a prerequisite for molecular materials, which serve as the active components in artificial photosynthesis solar cells and nanoscale devices [10–13]. Since the heterocyclic phenothiazine (PTZ) structure contains electron-rich sulfur and nitrogen heteroatoms, it is viewed as an excellent electron donor, which also exhibits remarkable photo-electron properties and potential commercial applications in organic light-emitting diodes (OLEDs) [14,15], photovoltaic cells [16,17] and organic integrated circuit sensors [18].

A fullerene-phenylphenothiazine compound, using *N*-hexyl phenothiazine, has been designed and synthesized experimentally [19]. For the donor-bridge-acceptor (D-π-A) system, there are two possible charge transfer (CT) processes: one is the sequentially jumped charge transfer process from the donor part to the bridge, and then from the bridge to the acceptor. Hence the jumping ICT process can proceed through bridging states as either real or virtual intermediated states; the other is the superexchange process, in which indirect long-distance electron transfer is enhanced by the mixture of the donor and the acceptor wave functions by way of the orbitals located between the donor and acceptor, and the CT process does not allow charge accumulation in a bridged state.

* Corresponding author. College of Science, Northeast Forestry University, Harbin 150040, PR China. Tel.: +86 451 82192245 8211.
E-mail address: yuanzuo.li@yahoo.com.cn (Y. Li).

0143-7208/$ – see front matter © 2011 Elsevier Ltd. All rights reserved.
doi:10.1016/j.dyepig.2011.08.017

Much effort has been made to understand the excited behavior of fullerene derivatives theoretically and experimentally [20–25]. Aswal et al. synthesized diodes based on donor–acceptor bilayers including fullerene (C60) and a tetraphenyl porphyrin derivative, and their work demonstrated that the C60 layer formed a supramolecular complex with the derivative and explained the rectification behavior with *ab initio* molecular-orbital theory [22]. Zandler reported recent research on the geometrical, spectral and electrochemical properties of molecular and supramolecular porphyrin-fullerene conjugates using the density functional theory (DFT) method [23]. Petsalakis et al. studied hybrid systems (dyads of fulleropyrolidine combined with pyrene, dithiapyrene, tetrathiofulvalene and porphyrin) with DFT and TD-DFT methods [24]. Chakrabarti et al. used the developed long-range corrected function to calculate the absorption spectrum of the fullerene-buckycatcher supramolecule and revealed the importance of the π-stacked interaction in controlling the absorption properties of the objective system [25].

It is important to gain understanding of the charge transfer microscopic mechanism of fullerene derivatives owing to their potential applications in molecular devices. Recently, several elaborate theoretical approaches have been developed, which consider all molecular orbitals contributing to the excitation of conjugated polymers [26,27] and stacking dimer systems [28]. The combination of quantum chemistry calculations with visual real-space analysis constitutes a powerful tool for the investigation of ICT and the excited states of organic molecules [26–31] and provides valuable information for further designing efficient molecular devices. In the present work, the photo-induced ICT and excited properties of a fullerene-phenylphenothiazine compound have been determined by using the TDDFT method as well as 2D–3D real-space analysis, in which the Coulomb attenuating method B3LYP (CAM-B3LYP) combining the hybrid qualities of B3LYP and long-range correction is used in our calculation. The mechanism of ICT in the fullerene, phenylphenothiazine (Ph-PTZ) and fullerene-phenylphenothiazine (Fullerene-Ph-PTZ) is also investigated.

Table 1
Transition energies (TE), oscillator strengths (Os) and CI main coefficient for phenyl-phenothiazine (Ph-PTZ) dyad.

	TE (nm)	λ_{max}[a] (nm)	Os (a.u)	CI main coefficient
S_1	302.37	320	0.0813	(0.58920)H → L
S_2	272.26		0.1041	(0.59528)H → L + 1
S_3	263.14	268	0.1510	(0.57970)H → L + 2

[a] The experimental data is from Ref. [19].

2. Methods

A fullerene-phenylphenothiazine compound has been reported experimentally in Ref. [19]. We performed quantum chemistry calculation together with real-space analysis to study the excited properties of the compound and charge transfer mechanism during photoexcitation. The molecular structures of fullerene, Ph-PTZ and fullerene-Ph-PTZ are shown in Fig. 1. The equilibrium geometry optimization for the ground state was obtained with density functional theory (DFT) [32], using the B3LYP functional [33] and 6-31G (d) basis sets. The transition energies and oscillator strengths in absorption were calculated with time dependent density functional theory (TD-DFT) [34], using the Cam-B3LYP [35] and 6-31G (d) basis sets. All the quantum chemical calculations were carried out using the Gaussian 09 suite [36]. It was assumed that the *N*-hexyl side group primarily affects compound solubility and conformation, but not directly the electronic structure of the conjugated backbone, this was left out of the calculations [13]. The density of state (DOS) and absorption spectra were studied with GaussSum 1.0 [37]. The excited state properties of these were investigated using 2D and 3D real space analysis. Briefly, in the 2D real-space analysis of transition density matrix, photo-excitation creates an electron-hole pair or an exciton by moving an electron from an occupied orbital to an unoccupied orbital [30,31], and

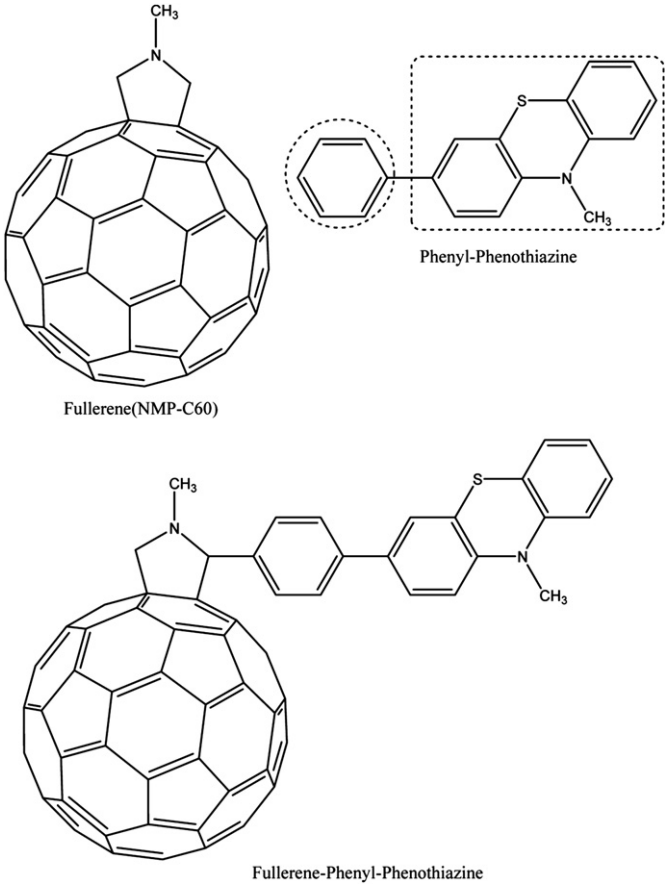

Fig. 1. Molecular structures of fullerene-phenyl-phenothiazine and reference compounds.

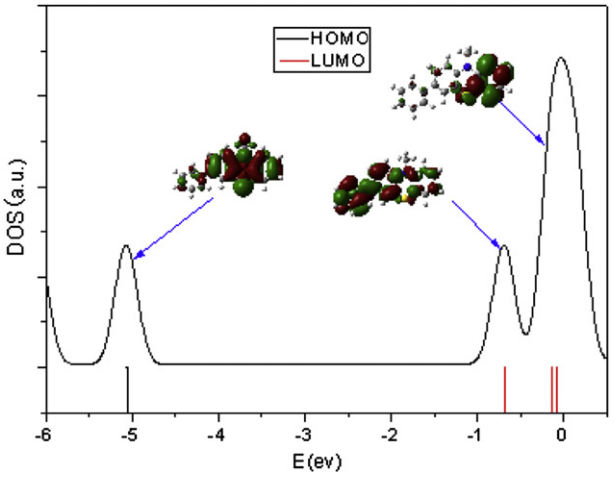

Fig. 2. DOS of phenyl-phenothiazine dyad, which shows shape and energies of HOMO and LUMO and LUNO + 2, respectively.

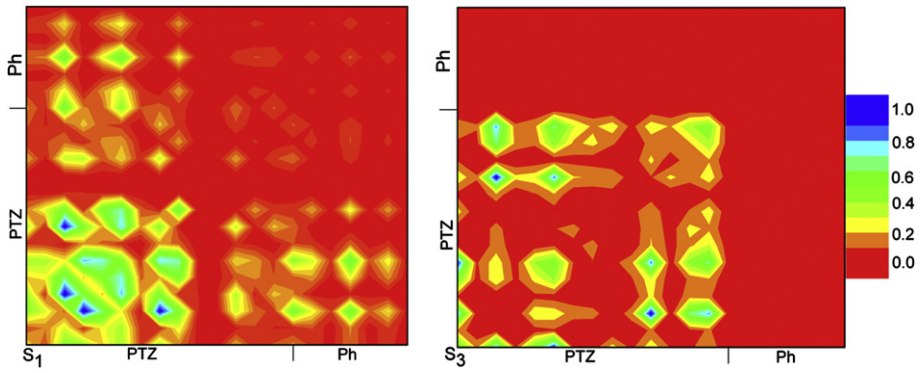

Fig. 3. The contour plots of transition density matrix of phenyl-phenothiazine dyad. The color bar is shown (absolute values of matrix elements, scaled to a maximum value of 1.0).

probability amplitudes $\psi(q,r)$ describe the charged particle in atomic orbital q on site x and the second in atomic orbital r on site y.

$$|\Psi(x,y)|^2 = \sum_{q\in x}\sum_{r\in y}|\psi(q,r)|^2 \quad (1)$$

where each element of transition density matrix $|\psi(q,r)|^2$ reflects the dynamics of this exciton projected on a pair of atomic orbitals given by its indices [30]. In the 3D real-space analysis, the charge difference density (CDD) shows the orientation and results of the charge and energy transfer [26–29].

$$\Delta\rho_{\mu\mu}(\vec{r}) = \sum_{\substack{a\in \text{unocc}\\ i,j\in \text{occ}}} C_{\mu aj}C_{\mu ai}\varphi_j(\vec{r})\varphi_i(\vec{r}) - \sum_{\substack{a,b\in \text{unocc}\\ i\in \text{occ}}} C_{\mu bi}C_{\mu ai}\varphi_b(\vec{r})\varphi_a(\vec{r}) \quad (2)$$

where C_{uai} represents the uth eigenvector of the configuration-interaction (CI) Hamiltonian based on the single-excitations from the occupied Hartree–Fock molecular orbital $\varphi_i(\vec{r})$ to the unoccupied one $\varphi_a(\vec{r})$. The first and the second terms in Eq. (2) stand for hole and electron in the CDD.

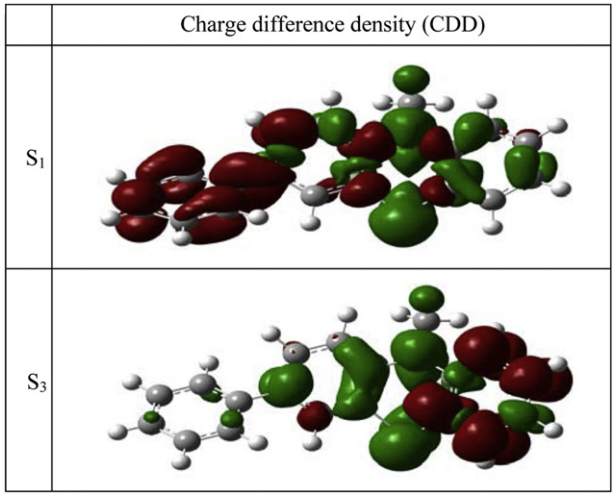

Fig. 4. Charge difference densities of phenyl-phenothiazine dyad, where green and red colors represent hole and electron densities, respectively (For interpretation of the references to color in this figure legend, the reader is referred to the web version of this article.).

3. Results and discussion

3.1. Electronic structure and excited state properties of phenyl-phenothiazine

Calculated transition energies and the oscillator strengths are listed in Table 1. The electronic structure and excited state properties of Ph-PTZ are studied with atom-resolved density of state (DOS, see Fig. 2), which shows the electron density distributions and energy levels of HOMO, LUMO and LUMO + 2, respectively. It is clearly shown in Fig. 2 that the electron density is significantly delocalized on the PTZ fragment for the HOMO, and the electron density of the LUMO is mainly populated on the phenyl (Ph) fragment; whereas the electron density of LUMO + 2 is localized on the phenothiazine (PTZ) benzene moiety. Therefore, this result suggests that the S_1 excited state (the HOMO–LUMO excitation) would shift the electron density distribution from the PTZ fragment to the Ph fragment, and this constitutes intramolecular charge transfer (ICT). The S_2 excited state has a similar result with the S_1 excited state; while for the S_3 state, the orbital transition (HOMO → LUMO + 2) results in a localized excited (LE) state.

From the contour plot of transition density matrix in Fig. 3, the electron-hole pairs are delocalized along the off-diagonal elements, which mean that there is electron-hole coherence between the PTZ and Ph fragments for the S_1 state, so this is an ICT excited state. To show the orientation of the ICT, charge difference density (CDD) was employed. From charge difference density in Fig. 4, we can see

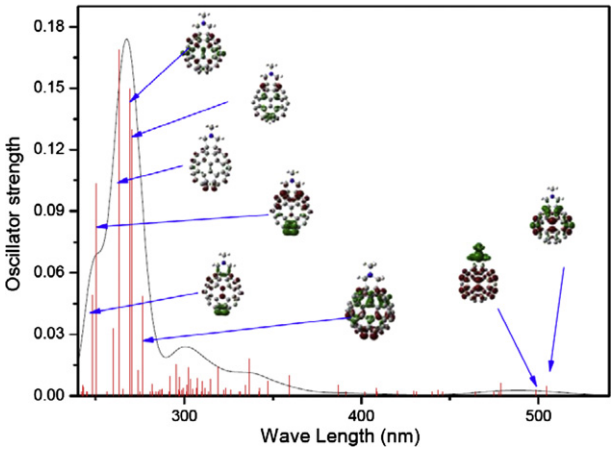

Fig. 5. The calculated absorption spectroscopy of fullerene, where the full width at half-maximum of the Gaussian curves is set 2000 cm^{-1}.

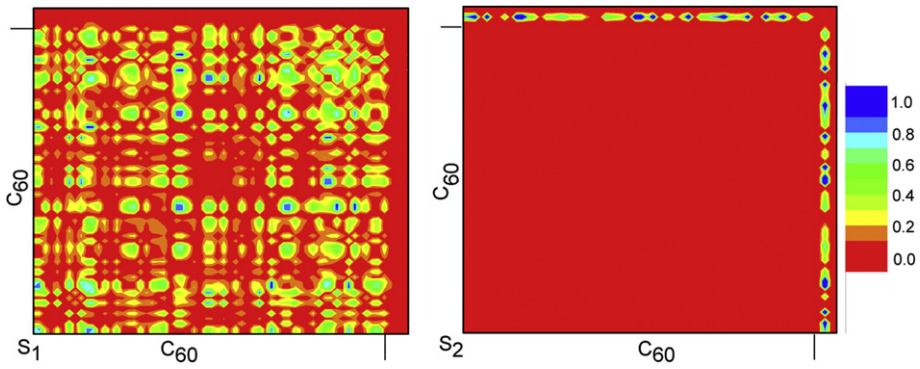

Fig. 6. The contour plots of transition density matrix of fullerene. The color bar is shown (absolute values of matrix elements, scaled to a maximum value of 1.0).

that the S_1 state electrons (red color) are mainly localized on the Ph fragment and holes (green color) are distributed over the PTZ fragment. Consequently, electron transfer occurs from PTZ to Ph (i.e. from donor to acceptor), producing the form of D^+A^-. Furthermore, the contour plot of transition density matrix in Fig. 3 also shows that the S_3 state is a locally excited state (D^*A), and here the electron-hole pairs upon photo-excitation are localized on the PTZ fragment. The charge difference density (see Fig. 4) not only reveals that S_3 is a localized excited state for PTZ-Ph dyad, but also reveals that for the PTZ fragment it is a localized ICT excited state, since the electron transfers from the one side of PTZ subunit to the terminal group.

3.2. Electronic structure and excited state properties of fullerene

The calculated transition energies and oscillator strengths for the seventy-five excited states are depicted in Fig. 5, which shows that the strong absorptions in the UV–vis spectrum are centered at 330 nm and 260 nm, respectively. The visible light region is characterized by relatively weak electron transitions, and the calculated first excited state in the absorption is at ~ 505 nm.

The excited state properties of some important excited states are identified with the 2D contour plot of transition density matrix and the 3D charge difference density. The real-space analysis shows that there are two kinds of excited state properties for the fullerene fragment upon excitation: one is the ICT excited state and the other is the LE state. The S_1 and S_2 states (at ~ 500 nm, see Fig. 5) can stand for these two types of excited state properties, respectively. The contour plots of the transition density matrix are given in Fig. 6, from which it can be seen that the first excited state is the locally excited state, where the electron-hole pairs are all localized on the C60 subunit; while for the second excited state, the red color resides in the C60 subunit and the green holes in the *N*-methylpyrrolidone (NMP) subunit upon excitation, and this result of the real-space analysis suggests that excitation would shift electron density redistribution from NMP to C60 subunit (see Fig. 6). Therefore, the S_2 state exhibits an ICT character.

3.3. Excited state properties of fullerene-phenylphenothiazine

The calculated transition energies and oscillator strengths of the fullerene-Ph-PTZ compound are listed in Table 2. The first excited state (S_1) is mainly contributed to the electron transition from HOMO to LUMO. Fig. 7 shows the shape and energies of HOMO and LUMO. The electron densities of HOMO and LUMO are totally localized on the PTZ and the fullerene fragments, which mean that the PTZ and fullerene fragments act as an electron-donor and an electron-acceptor, respectively, so the S_1 state is the ICT state. The introduction of donor group (PTZ) caused charge redistribution in the fullerene fragment and reduced the HOMO–LUMO energy gap (ΔE_{H-L}). The ΔE_{H-L} of the fullerene-Ph-PTZ compound (1.823 eV) was lower than that of fullerene fragment (2.721 eV), which indicates that the electrons are easy to transfer from the occupied orbitals of donor to the virtual orbital of the acceptor.

Transition density matrix and charge difference density (CDD) reveal the orientation of charge transfer and excited state properties of the fullerene-phenylphenothiazine compound. In this paper, only five important excited states are shown in Figs. 8 and 9, which

Table 2
The transition energies (TE), oscillator strengths (Os), transition dipole moments and excited state properties of Fullerene-Ph-PTZ compound.

	TE/Os	Transition dipole moments			Excited state properties
	(nm, a.u)	X (a.u)	Y (a.u)	Z (a.u)	
S_1	517.63 (0.0033)	−0.1836	−0.1434	0.0487	ICT (PT → F)
S_2	500.47 (0.0000)	0.0219	0.0082	0.0004	ICT (PT → F)
S_3	492.47 (0.0000)	0.0131	0.0012	−0.01	ICT (PT → F)
S_4	490.45 (0.0000)	0.0013	0.0019	0.0138	ICT (PT → F)
S_5	454.15 (0.0003)	0.0538	0.0408	−0.0136	ICT (F)
S_6	445.46 (0.0001)	−0.0222	0.0306	0.0004	LE (F)
S_7	443.00 (0.0000)	−0.0134	−0.0004	−0.0078	LE (F)
S_8	434.50 (0.0003)	−0.0529	0.0382	−0.0187	LE (F)
S_9	422.60 (0.0013)	−0.0587	−0.0092	−0.1216	LE (F)
S_{10}	412.12 (0.0016)	0.1458	−0.0248	0.019	LE (F)
S_{11}	408.92 (0.0000)	0.0045	0.0029	−0.0037	LE (F)
S_{12}	407.23 (0.0002)	0.0012	−0.0084	−0.0538	LE (F)
S_{13}	386.09 (0.0031)	−0.0289	−0.0199	−0.1952	ICT (PT → F)
S_{14}	383.93 (0.0002)	0.0139	−0.0076	−0.0461	LE (F)
S_{15}	370.52 (0.0143)	0.3128	0.2595	−0.093	ICT (PT-P → F)
S_{16}	358.70 (0.0051)	0.2316	0.0774	−0.0283	ICT (PT → F)
S_{17}	358.14 (0.0003)	0.0332	−0.0454	0.0067	ICT (F)
S_{18}	350.01 (0.0000)	−0.0173	−0.0062	0.013	ICT (PT → F)
S_{19}	346.97 (0.0002)	0.0313	−0.025	−0.0223	LE (F)
S_{20}	344.72 (0.0066)	−0.2727	−0.0031	−0.0026	LE (F)
S_{21}	332.31 (0.0009)	−0.02	0.0887	0.0385	ICT (PT-P → F)
S_{22}	332.07 (0.0008)	0.0874	−0.0167	−0.0241	ICT (PT → F)
S_{23}	329.79 (0.0188)	0.0657	0.0649	0.4426	LE (F)
S_{24}	327.26 (0.0054)	0.183	−0.1223	0.0996	LE (F)
S_{25}	322.54 (0.0000)	−0.0089	−0.0049	−0.0177	ICT (PT-P → F)
S_{26}	318.56 (0.0054)	−0.0263	−0.0217	−0.2353	ICT (PT-P → F)
S_{27}	317.60 (0.0020)	0.1335	0.0367	0.042	ICT (PT → F)
S_{28}	315.32 (0.0002)	−0.0138	0.033	−0.035	LE (F)
S_{29}	306.23 (0.0265)	0.2431	0.4233	−0.1698	LE (F)
S_{30}	304.66 (0.2365)	−1.496	−0.3649	0.0167	ICT (P → F)
S_{31}	303.10 (0.0028)	−0.1181	−0.1127	0.0347	ICT (PT-P → F)
S_{32}	299.92 (0.0116)	−0.2671	−0.1996	0.062	ICT (F)
S_{33}	299.60 (0.0036)	0.153	−0.0581	−0.0916	ICT (P → F)
S_{34}	295.18 (0.0003)	−0.0319	0.0305	−0.0299	ICT (PT-P → F)
S_{35}	293.03 (0.0082)	−0.1739	0.0171	−0.2204	ICT (P → F)

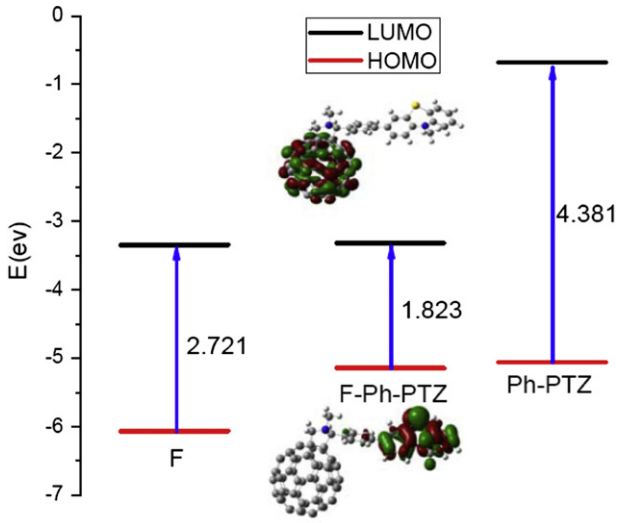

Fig. 7. The molecular orbital energy levels of the HOMO and LUMO for Fullerene, Ph-PTZ dyad and Fullerene-Ph-PTZ compound.

stand for the different types of excited state properties. It is shown clearly in Fig. 9 that electron-hole coherences are mainly between C60 and PTZ fragments for the S_1 state, as supported by CDD analysis in Fig. 8. For this state photo-excitation would move an electron to the C60 subunit (see Fig. 8). Meanwhile, we also found that there are similar results for the S_1–S_4, S_{13}, S_{16}, S_{18}, S_{22} and S_{27} states. Photoinduced electron transfer directly takes place from PTZ to C60, without passing through the bridge (tunneling through the bridge), which is characterized as the D^+BA^- form, so the ICT mechanism for those states is the superexchange mechanism.

For S_{30}, S_{33} and S_{35} states, the charge difference densities show the electrons on the C60 subunit are only donated from the Ph fragment without from PTZ fragment, since the holes are mainly localized on the Ph fragment. Those states are also ICT states (D^+B^-A), and the Ph fragment takes the role of the week donor. The strong ICT states have taken place upon photo-excitation, corresponding to the S_{15}, S_{21}, S_{25}, S_{26}, $S_{31}$and S_{34} states. Here, holes are localized on the Ph fragment and the PTZ fragment, respectively; while electrons are localized on the C60 subunit. Electron transfer can pertain to the form of the D–B fragments to the A fragment. Furthermore, it is worth noting that there are similar results for the excited states S_5, S_{17} and S_{32}, which are also the ICT excited states where electron transfer occurs in the fullerene fragment (i.e. the charges transfer from the NMP to the C60 subunit). The process is similar to the case of the fullerene monomer. From the charge difference densities, the S_6–S_7, S_8–S_{12}, S_{14}, S_{19}–S_{20}, S_{23}–S_{24} and S_{28}–S_{29} states are the locally excited (LE) states, where the holes and electrons are all localized on the C_{60} subunit (see Fig. 8). The electron-hole coherence of the S_7 state can be seen from Fig. 9, where the electron-hole pairs are localized on the fullerene subunit.

Electronic coupling elements of electron transfer in D–π–A system is one of the key parameters that determine the rate of charge transfer through the fullerene-Ph-PTZ compound, which can be calculated by using the generalized Mulliken-Hush or fragment charge methods [38]. In the two-state (S_0 and S_i states, $i = 1, 2, \ldots$) formulation,

$$H_{ab} = \frac{\mu_{tr}\Delta E}{\sqrt{(\Delta\mu)^2+4(\mu_{tr})^2}} \tag{3}$$

This expression involves the energy difference ΔE and transition dipole moment μ_{tr} (see Table 2), as well as the corresponding

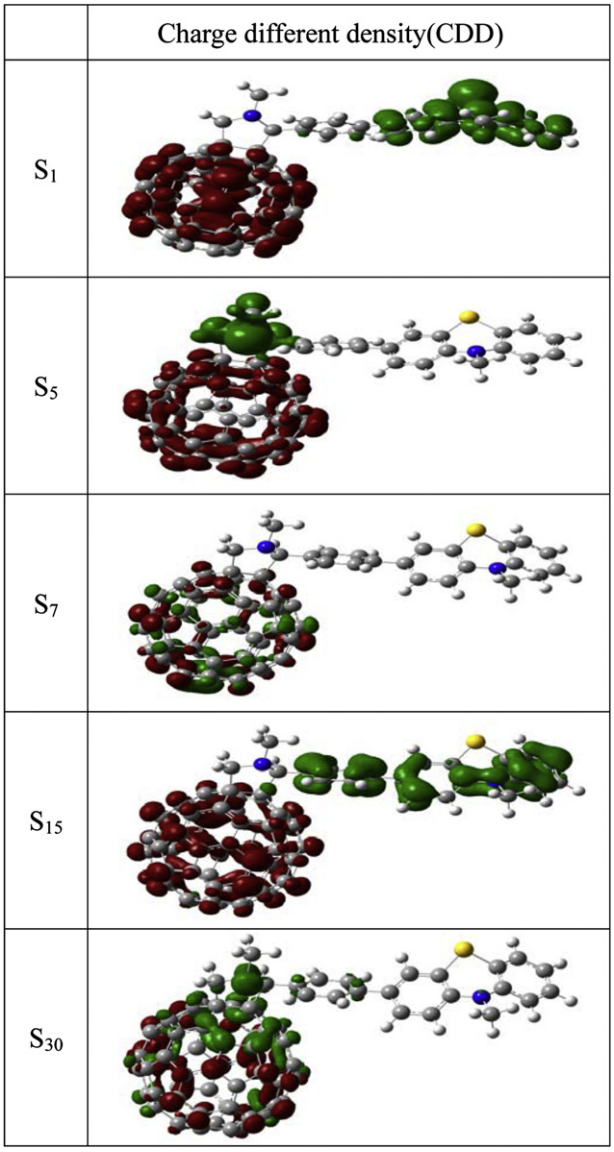

Fig. 8. Charge difference densities of Fullerene-Ph-PTZ, where green and red colors represent hole and electron densities, respectively (For interpretation of the references to color in this figure legend, the reader is referred to the web version of this article.).

dipole moment difference $\Delta\mu$, between the initial and final electronic states. The dipole moment difference in the above equation could be calculated by using the Hellmann–Feynman theorem, as the analytical derivative of the excited-state energy with respect to an applied electric field. The dipole moments of excited states are estimated by using a finite field strategy (orientation is along CT direction). The transition energy dependent on the static electric field F can be expressed as [39],

$$E_{exc}(F) = E_{exc}(0) - \Delta\mu F - \frac{1}{2}\Delta\alpha F^2 \tag{4}$$

where $E_{exc}(0) = \Delta E$ is the excitation energy at zero field, $\Delta\alpha$ is the change in polarizability. We calculated the typical five states, and the fitted values of $\Delta\mu$ for the S_1, S_5, S_7, S_{15} and S_{30} states are 0.25 au, 5.098 au, 0.1 au, 0.475 au and 0.045 au, respectively. According to equation (3), the electronic coupling element (H_{ab}) is calculated to be the value of 0.08813 au (12,090 meV), 0.1004 au (28.57 meV), 0.1029 au (362.4 meV), 0.1231 au (15,100 meV), 0.1499 au

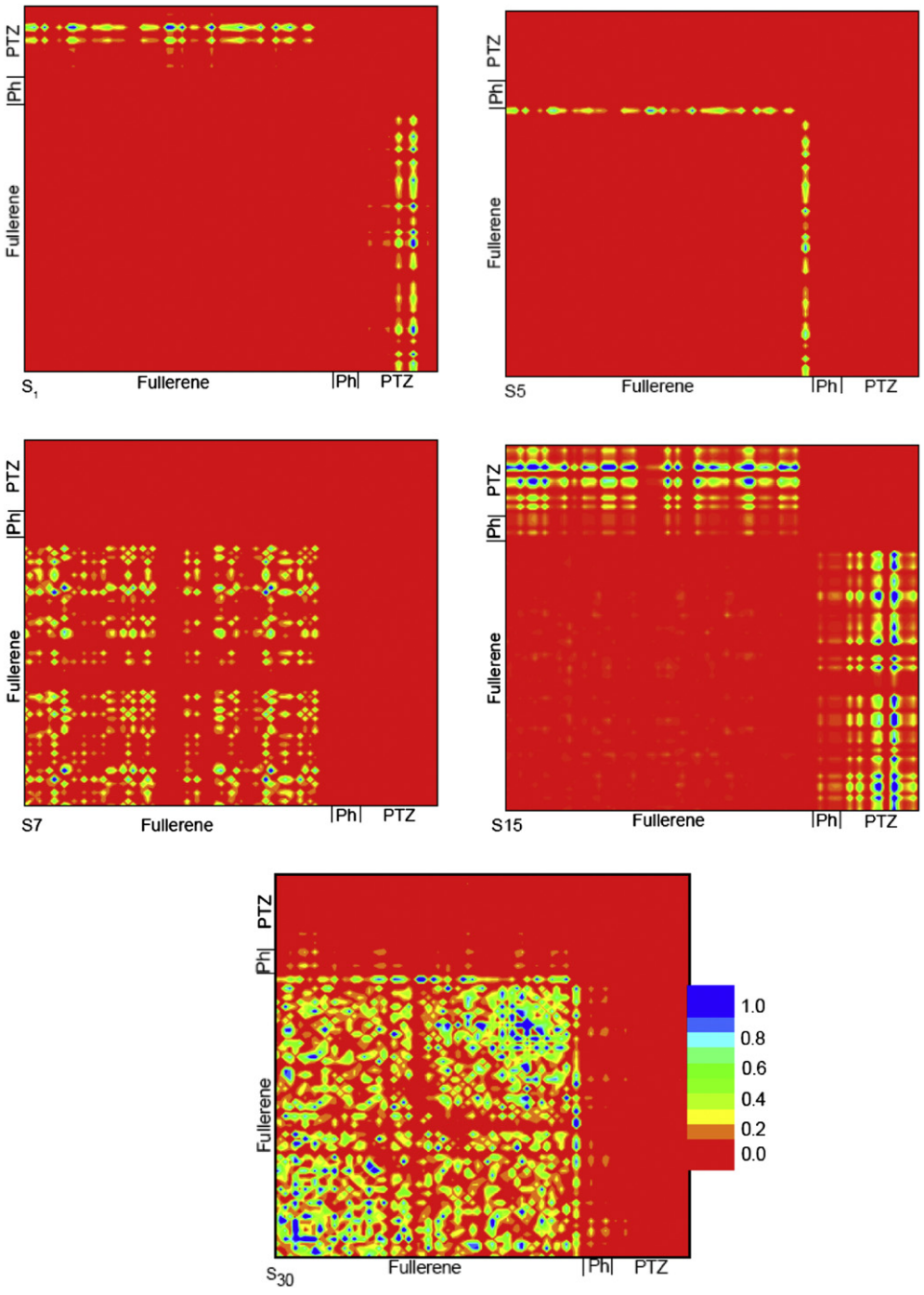

Fig. 9. The contour plots of transition density matrix of Fullerene-Ph-PTZ. The color bar is shown (absolute values of matrix elements, scaled to a maximum value of 1.0).

(2039 meV), respectively. Calculated values of H_{ab} are in this order $H_{15} > H_1 > H_{30} > H_7 > H_5$. From the proportional relationship between ET rate constant and electronic coupling element [40], it is understandable that the ET rate from the ground state to the S_{15}, S_1, and S_{30} states can be predicted much faster than that to the S_7 and S_5 states. From the CDD in Fig. 8 and excited properties in Table 2, we found that the S_{15}, S_1, and S_{30} states are all ICT states, in which donor and acceptor units have a strong coupling effect due to the distribution character of electron-hole pairs; while for the S_7 and S_5 states, they are locally excited states in fullerene units. These results enable us to make a prediction that the electron transfer process for ICT state more easily takes place than locally excited states process owing to the relatively higher electronic coupling effects. Moreover, for S_{15} state donor-bridge-acceptor fragments have strong coupling effects, and CT processes of this state most often occur among the calculated CT states, and for this state more electrons are transferred from the phenylphenothiazine unit to the fullerene unit (see Fig. 8).

4. Conclusion

The equilibrium geometries and electron structures of the fullerene, phenylphenothiazine and fullerene-phenylphenothiazine have been studied by using quantum chemical methods combined

with real-space analysis. With the visualized methods, four charge transfer (CT) ways have been revealed for the calculated excited states, in which the direct superexchange ICT process (tunneling through the phenyl unit) has been found in the fullerene-phenylphenothiazine system. Through the analysis of electronic coupling matrix element and charge transfer densities for some states, it is found that the superexchange CT and the direct CT more easily occur than the locally excited state in the fullerene fragment during the primary photoexcitation.

Acknowledgements

This work was supported by the National Natural Science Foundation of China (Grant Nos: 10604012, 20703064 and 10874234) and the Fundamental Research Funds for the Central Universities (Grant No: DL12BB19).

References

[1] Balzani V, Moggi L, Manfrin MF, Bolletta F, Gleria M. Solar energy conversion by water photodissociation transition metal complexes can provide low-energy cyclic systems for catalytic photodissociation of water. Science 1975; 189:852–6.
[2] Calvin M. Simulating photosynthetic quantum conversion. Acc Chem Res 1978;10:369–74.
[3] Bryce MR. Tetrathiafulvalenes as π-electron donors for intramolecular charge-transfer materials. Adv Mater 1999;11:11–23.
[4] Polivka T, Sundstrom V. Ultrafast dynamics of carotenoid excited states-from solution to natural and artificial systems. Chem Rev 2004;104:2021–71.
[5] Wang XF, Xiang JF, Wang P, Koyama Y, Yanagida S, Wada Y, et al. Dye-sensitized solar cells using a chlorophyll *a* derivative as the sensitizer and carotenoids having different conjugation lengths as redox spacers. Chem Phys Lett 2005;408:409–14.
[6] Yu G, Gao J, Hummelen JC, Wudl F, Heeger AJ. Polymer photovoltaic cells: enhanced efficiencies via a network of internal donor-acceptor heterojunctions. Science 1995;270:1789–91.
[7] Thomas KG, Biju V, Guldi DM, Kamat PV, George MV. Orientation dependent electron transfer processes in Fullerene-Aniline Dyads. J Phys Chem A 1999; 103:10755–63.
[8] Guldi DM, Prato M. Excited-state properties of C_{60} fullerene derivatives. Acc Chem Res 2000;33:695–703.
[9] Fujitsuka M, Matsumoto K, Ito O, Yamashiro T, Aso Y, Otsubo T. Pico- and nano-second laser flash photolysis study on photoinduced charge separation in oligothiophene-C_{60} dyad molecules. Res Chem Intermed 2001;27:73–88.
[10] Martinez-Diaz MV, Fender N, Rodriguez-Morgade MS, Gomes-Lopes M, Dietrich F, Echioyen L, et al. A supramolecular approach for the formation of fullerene–phthalo cyanine dyads. J Mater Chem 2002;12:2095–9.
[11] Van hal PA, Knol J, Langeveld-Voss BMW, Meskers SCJ, Hummelen JC, Janssen RAJ. Photoinduced energy and electron transfer in fullerene–oligothiophene– fullerene triads. J Phys Chem A 2000;104:5974–88.
[12] Ikemoto J, Takimiya K, Aso Y, Otsubo T, Fujitsuka M, Ito O. Porphyrin– oligothiophene–fullerene triads as an efficient intramolecular electron-transfer system. Org Lett 2002;4:309–11.
[13] Sun MT, Chen YH, Song P, Ma FC. Intramolecular charge transfer and locally excited states of the fullerene-linked quarter-thiophenes dyad. Chem Phys Lett 2005;413:110–7.
[14] Alam MM, Jenekhe SA. Polybenzobisazoles are efficient electron transport materials for improving the performance and stability of polymer light-emitting diodes. Chem Mater 2002;14:4775–80.
[15] Shen Z, Procházka R, Daub J, Fritz N, Acar N, Schneider S. Towards modelling light processes of blue-light photoreceptors. Pyrene-isoalloxazine (flavin)-phenothiazine triad: electrochemical, photophysical, investigations and quantum chemical calculations. Phys Chem Chem Phys 2003;5:3257–69.
[16] Tian HN, Yang XC, Chen RK, Pan YZ, Li L, Hagfeldt A, et al. Phenothiazine derivatives for efficient organic dye-sensitized solar cells. Chem Commun; 2007:3741–3.
[17] Alam MM, Jenekhe SA. Nanolayered heterojunctions of donor and acceptor conjugated polymers of interest in light emitting and photovoltaic devices: photoinduced electron transfer at polythiophene/polyquinoline interfaces. J Phys Chem B 2001;105:2479–82.
[18] Arshak K, Morris D, Arshak A, Korostynska O, Jafer E, Waldron D, et al. Development of polymer-based sensors for integration into a wireless data acquisition system suitable for monitoring environmental and physiological processes. Biomol Eng 2006;23:253–7.
[19] Bucci N, Müller TJJ. Synthesis and electronic properties of (oligo)phenothiazine -ethynyl-hydro-C-60 dyads. Tetrahedron Lett 2006;47:8323–7.
[20] Komamine S, Fujitsuka M, Ito O, Itaya A. Photoinduced electron transfer between C_{60} and carbazole dimer compounds in a polar solvent. J Photochem Photobiol A Chem 2000;135:111–7.
[21] Sandanayaka ASD, Araki Y, Ito O, Deviprasad GR, Smith PM, Rogers LM, et al. Photoinduced electron transfer in fullerene triads bearing pyrene and fluorene. Chem Phys 2006;325:452–60.
[22] Koiry SP, Jha P, Aswal DK, Nayak SK, Majumdar C, Chattopadhyay S, et al. Diodes based on bilayers comprising of tetraphenyl porphyrin derivative and fullerene for hybrid nanoelectronics. Chem Phys Lett 2010;485:137–41.
[23] Zandler ME, D'Souza F. The remarkable ability of B3LYP/3-21G (d) calculations to describe geometry, spectral and electrochemical properties of molecular and supramolecular porphyrin-fullerene conjugates. Comp Rendus Chim 2006;9:960–81.
[24] Petsalakis ID, Theodorakopoulos G. Photoinduced charge transfer in fullerene– donor dyads: a theoretical study. Chem Phys Lett 2008;466:189–96.
[25] Chakrabarti S, Ruud K. Intermolecular Interaction-controlled tuning of the two-photon absorption of fullerene bound in a buckycatcher. J Phys Chem A 2009;113:5485–8.
[26] Sun MT, Kjellberg P, Beenken WJD, Pullerits T. Comparison of the electronic structure of PPV and its derivative DIOXA-PPV. Chem Phys 2006;327:474–84.
[27] Beenken WJD, Pullerits T. Spectroscopic units in conjugated polymers: a quantum chemically founded concept? J Phys Chem B 2004;108:6164–9.
[28] Li YZ, Li HX, Zhao XM, Chen MD. Electronic structure and optical properties of dianionic and dicationic π-dimers. J Phys Chem A 2010;114:6972–7.
[29] Sun MT, Ding Y, Li LW, Xu HX. Do coupling exciton and oscillation of electron-hole pair exist in neutral and charged π -dimeric quinquethiophenes? J Chem Phys 2007;127:084706–14.
[30] Tretiak S, Saxena A, Martin RL, Bishop AR. Conformational dynamics of photoexcited conjugated molecules. Phys Rev Lett 2002;89:097402–7.
[31] Mukamel S, Tretiak S, Wagersreiter T, Chernyak V. Electronic Coherence and collective optical excitations of conjugated molecules. Science 1997;277:781–7.
[32] Dreizler JMR, Gross EKU. Density functional theory. Heidelberg: Springer Verlag; 1990.
[33] (a) Becke AD. Density-functional exchange-energy approximation with correct asymptotic behavior. Phys Rev A 1988;38:3098–100;
(b) Becke AD. Density- functional thermochemistry. III. The role of exact exchange. J Chem Phys 1993;98:5648–52;
(c) Lee C, Yang W, Parr RG. Development of the colle-salvetti correlation-energy formula into a functional of the electron density. Phys Rev B 1998;37:785–9.
[34] Stratmann RE, Scuseria GE, Frisch MJ. An efficient implementation of time-dependent density-functional theory for the calculation of excitation energies of large molecules. J Chem Phys 1998;109:8218–24.
[35] Yanai T, Tew DP, Handy NC. A new hybrid exchange-correlation functional using the Coulomb-attenuating method (CAM-B3LYP). Chem Phys Lett 2004; 393:51–7.
[36] Frisch MJ, Trucks GW, Schlegel HB, Scuseria GE, Robb MA, Cheeseman JR, et al. Gaussian 09, revision A.02. Wallingford, CT: Gaussian, Inc.; 2009.
[37] O'Boyle NM, Vos JG. GaussSum 1.0. Dublin City University. Available at: http://gausssum.sourceforge.net; 2005.
[38] Wang Q, Newton MD. Structure, energetics, and electronic coupling in the $(TCNE_2)^-$ encounter complex in solution: a polarizable continuum study. J Phys Chem B 2008;112:568–76.
[39] Grozema FC, Telesca R, Jonkman HT, Siebbeles LDA, Snijders JG. Excited state polarizabilities of conjugated molecules calculated using time dependent density functional theory. J Chem Phys 2001;115:10011–4.
[40] Mikkelsen KV, Ratner MA. Electron tunneling in solid-state electron-transfer reactions. Chem Rev 1987;87:113–53.